Earth and Planetary Science Letters 373 (2013) 169–178

Contents lists available at SciVerse ScienceDirect

Earth and Planetary Science Letters

journal homepage: www.elsevier.com/locate/epsl

The Earth's core composition from high pressure density measurements of liquid iron alloys

G. Morard [a,*], J. Siebert [a], D. Andrault [b], N. Guignot [c], G. Garbarino [d], F. Guyot [a], D. Antonangeli [a]

[a] Institut de Minéralogie et de Physique des Milieux Condensés, UMR CNRS 7590, Université Pierre et Marie Curie, 75005 Paris, France
[b] Laboratoire Magmas et Volcans, Université Blaise Pascal, Clermont-Ferrand F-63006, France
[c] Synchrotron SOLEIL, Gif-sur-Yvette F-91192, France
[d] European Synchrotron Radiation Facility, Grenoble F-38043, France

ARTICLE INFO

Article history:
Received 6 November 2012
Received in revised form
18 April 2013
Accepted 27 April 2013
Editor: Y. Ricard
Available online 25 May 2013

Keywords:
Earth's core composition
high pressure
density
liquid iron alloys

ABSTRACT

High-pressure, high-temperature *in situ* X-ray diffraction has been measured in liquid iron alloys (Fe–5 wt% Ni–12 wt% S and Fe–5 wt% Ni–15 wt% Si) up to 94 GPa and 3200 K in laser-heated diamond anvil cells. From the analysis of the X-ray diffuse scattering signal of the metallic liquids, we determined density and bulk modulus of the two liquid alloys. Comparison with a reference Earth model indicates that a core composition containing 6% of sulfur and 2% of silicon by weight would best match the geophysical data. Models with 2.5% of sulfur and 4–5% of silicon are still consistent with geophysical constraints whereas silicon only compositions are not. These results suggest only moderate depletion of sulfur in the bulk Earth.

1. Introduction

The liquid core of the Earth extends between 2900 km and 5150 km depth accounting for 18% of the total planetary volume. Although mostly composed of iron, it contains impurities that lower its density and melting point with respect to pure Fe (Birch, 1964; Poirier, 1994). Knowledge of the nature and content in light elements (O, S, Si) in the core has major implications for establishing the bulk composition of the Earth, for determining the possibility of compositional convection in the outer core, itself closely related to generation of the Earth's magnetic field (Aubert et al., 2008). Furthermore, amount and nature of light elements present in the Earth's core are intimately linked with the scenario of Earth's differentiation. Composition of the metallic phase in equilibrium is important when trying to reconcile metal/silicate partitioning data with the current mantle abundances (Corgne et al., 2009; Siebert et al., 2012; Wade and Wood, 2005; Wade et al., 2012).

In order to discriminate between the different potential light elements, the most straightforward method should be to compare the physical properties of liquid iron alloys measured under pertinent pressure (P) and temperature (T) conditions with geophysical models of the Earth, such as PREM (Dziewonski and Anderson, 1981), which provide density (ρ) and longitudinal acoustic velocity (Vp) as a function of depth in the outer core, and the density jump at the inner–outer core boundary (IOCB).

Sulfur (S), silicon (Si) and oxygen (O) are traditionally listed as the most likely light elements entering in the composition of the Earth's core (Poirier, 1994). Each element has a specific effect on the iron phase diagram, melting temperature and melt properties, as well as on the structure of the liquid phase (Morard et al., 2008b), which could in principle be used to discriminate among them. For example, it has been shown that the bulk modulus measured in the 0–5 GPa pressure range decreases by 15% by addition of 10 wt% of S, whereas 10 wt% of Si have basically no effect (Sanloup et al., 2004). Accordingly, in this pressure range, the structure of the liquid is strongly modified by S while Si hardly modifies it (Morard et al., 2008b). Because the bulk modulus of the PREM model is quite close to that of pure Fe at high pressure and temperature, these low pressure results are not in favor of abundant S in the core. They cannot however be directly extrapolated to core pressures.

Due to difficulties in performing reliable density measurements on liquids at very high pressures, the composition of the solid Earth's inner core, which represents less than 1% of the volume of the Earth, has often been used as an indirect way to infer the composition of the liquid core. For instance, the low solubility of

* Corresponding author. Tel.: +33 1 44 27 52 22.
E-mail address: guillaume.morard@impmc.jussieu.fr (G. Morard).

0012-821X/$ - see front matter © 2013 Elsevier B.V. All rights reserved.
http://dx.doi.org/10.1016/j.epsl.2013.04.040

oxygen in solid iron at core conditions qualitatively correlates well with the density jump at the IOCB. This was used as an argument in favor of the presence of O in the liquid core (Alfè et al., 2002; Ozawa et al., 2008). Si and S could both enter as well in the composition of the Earth's solid inner core, in various combinations, as demonstrated by density and sound velocity measurements (Antonangeli et al., 2010; Badro et al., 2007; Sakai et al., 2012).

From a cosmochemical point of view, sulfur content in the Earth's core is estimated around 2 wt%, by comparing the depletion of sulfur in the Earth's mantle and the volatility trend (relative abundance of elements to chondritic composition versus condensation temperature) (Dreibus and Palme, 1995; McDonough, 2003). Moreover, equilibration between liquid silicates and liquid metal at the bottom of a magma ocean is thought to result in incorporation of high amounts of O and Si in the metallic phase (Siebert et al., 2012). However, cores of the parent bodies of iron meteorites are known to contain up to 17 wt% of S (Chabot, 2004), implying that S-rich differentiated materials could potentially enter into the Earth's formation process, and be a large source of S if cores of accreting planetesimals joined the Earth's core without further equilibration (Rudge et al., 2010).

Measurement of equations of state of liquid iron alloys, and comparison with reference Earth models in the outer core remain one of the most direct way to solve this dilemma. We thus undertook an experimental study of density and compressibility of liquid S-bearing and Si-bearing iron alloys, obtaining data up to 94 GPa and 3200 K. Details of data collection and analysis are reported in section 2, while obtained results are presented in Section 3 and their geophysical implications discussed in Section 4. Our main conclusions are summarized in Section 5.

2. Experimental methods

2.1. Laser-heated diamond anvil cell (LH-DAC) experiments

Starting materials were synthesized by an ultra-rapid quench method at the ICMPE (Institut de Chimie et des Matériaux de Paris-Est, Paris, France), for two compositions of Fe–5 wt%Ni–15 wt %Si, and Fe–5 wt%Ni–12 wt%S. Samples composition and homogeneity have been described in a previous paper (Morard et al., 2011). Both compositions included 5 wt% Ni, in agreement with all Earth's core geochemical models (Allègre et al., 1995). We expect however a negligible effect of Ni on the elastic properties and phase diagram of the metallic phases (Antonangeli et al., 2010; Komabayashi et al., 2012).

Angle dispersive X-ray diffraction experiments in double-sided laser heated diamond anvil cell (LH-DAC) were performed at ID27 beamline at the European Synchrotron Radiation Facility (ESRF) in Grenoble (Mezouar et al., 2005). Samples were heated on both sides by two continuous fibers YAG lasers (TEM 00) providing a maximum total power of 200 W. Temperatures were obtained from spectroradiometric method, using reflective collecting optics (Schultz et al., 2005). Laser spots were more than 20 μm in diameter. Temperature was measured at the center of the hot spot by analyzing the pyrometric signal emitted by a 2×2 μm^2 area. Heating power of the two lasers was tuned in order to obtain a same temperature on both sample sides.

High pressures were generated with Le Toullec-type diamond anvil cells equipped with diamonds with 250, 300 lm flat or 150/300 lm bevelled diameter culets. Diamonds with conical supports (Boehler and De Hantsetters, 2004) were used in order to collect X-ray diffraction over a wide 2-theta angle (70°). The metallic foils were crushed in an agate mortar, and flakes with a thickness of ~10 μm and a diameter of ~50 μm were selected. These specimens were loaded between two dry KCl layers in 50–100 μm diameter holes drilled in a preindented rhenium gasket. KCl acts as a soft pressure medium at high temperature, insuring good hydrostatic conditions, with the further advantage of being chemically inert with the iron alloys (no reaction between KCl pressure medium and Fe liquid alloys has been noted from the analysis of quenched samples diffraction patterns). It also presents the property of trapping the melt, which enables the possibility of collecting a good X-ray diffraction signal. Furthermore, using KCl insulating layers seems to limit migration of elements by Soret effects in the laser spot (Sinmyo and Hirose, 2010).

In situ investigations enable determination of melting temperature (Morard et al., 2011) and structural and density properties of the liquid alloys. Experiments were performed on the Fe–Ni–S alloy up to 94 GPa and 2800 K and on the Fe–Ni–Si alloy up to 91 GPa and 3200 K. Thanks to the stability of lasers and to the precision of temperature measurements, we could control ~50 K step increases in temperature. Diffraction patterns were recorded at each temperature step with 10–30 s integration times. Liquid diffraction patterns were acquired when complete melting was achieved (~200 K above melting point for Fe–Si alloys; ~500 K above melting point for Fe–S alloys). Pressure is determined at ambient conditions using KCl equation of state (Walker et al., 2002) and empirical law is used to estimate thermal pressure (Andrault et al., 1998). Experimental details have been described in a previous publication (Morard et al., 2011).

2.2. Data processing

Density of liquid phases at elevated pressures can be investigated using *in situ* or *ex situ* techniques. The most common are respectively the measurements of the X-ray absorption profile (Sanloup et al., 2004, 2000; Terasaki et al., 2010) or the sink/float methods (Balog et al., 2003; Nishida et al., 2008). However, these methods suffer several limitations. The *ex situ* sink/float techniques cannot be applied to laser-heated diamond anvil cells (LH-DAC), as they require large samples. Furthermore, the sample density can only be bracketed between those of falling spheres made of different materials, thus leading to large uncertainties. For the X-ray absorption technique, the major limitation is the knowledge of the sample geometry. DAC samples are a few tens of microns diameter, and even less in thickness, and their 3-dimension geometry is particularly difficult to measure precisely, especially at very high pressure, when diamonds significantly deform.

In this paper, we follow a procedure, originally developed by Kaplow et al. (1965), and applied to liquid water and argon compressed in diamond anvil cell (Eggert et al., 2002): (1) Diffuse scattering from the liquid sample (above melting point) and from the background (below melting point, dominated by the Compton contribution of the diamonds) are fitted using Igor Pro software (Fig. 1). (2) After subtraction of the background signal, liquid scattering signal is normalized to obtain the scattering factor $S(Q)$. (3) An iterative procedure is then applied to calculate the pair distribution function $g(r)$, as well as the density of the liquid alloy.

The numerical procedure employed for the analysis of the diffuse signal from the liquid iron alloys in LH-DAC is detailed in Appendix A. Here we briefly review the main steps, basics assumptions and sources of uncertainties.

The signal scattered by the liquid $I_S(Q)$ is obtained by subtraction of the background signal $I_{bk}(Q)$ obtained before melting to the high temperature measured signal $I_{meas}(Q)$ (Fig. 1). These scattering signals are carefully fitted in order to remove the solid phase diffraction peaks (KCl or solid metal in equilibrium with the liquid) using the software Igor Pro. Differently than what was done in previous experiments in Paris Edinburgh press (Morard et al., 2008a), fits are performed on the raw diffraction signal, before background subtraction. Here, this subtraction is adjusted through

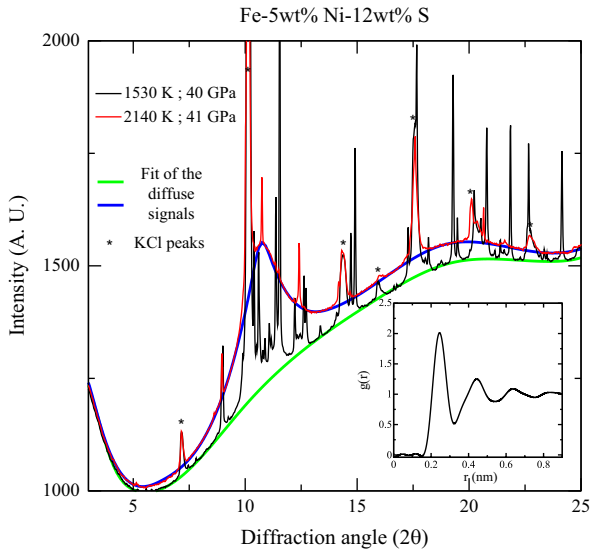

Fig. 1. Diffraction patterns of liquid (2140 K, 41 GPa) and solid (1530 K, 40 GPa) Fe–5 wt%Ni–12 wt% S alloy and the corresponding fit used for density determination. After removal of Bragg diffraction peaks from solids, the diffuse scattering signals are shown in green and blue for the spectra of solid and liquid, respectively. Inset: pair distribution function $g(r)$ of the liquid obtained after the data treatment procedure. (For interpretation of the references to color in this figure legend, the reader is referred to the web version of this article.)

a scale factor b:

$$I_S(Q) = I_{meas}(Q) - bI_{bk}(Q) \quad (1)$$

Next, the signal is normalized using the Krogh-Moe–Norman method (Krogh-Moe, 1956; Norman, 1957) in order to obtain the structure factor $S(Q)$. Then, by Fourier transform of $S(Q)$, one obtains the distribution function $F(r)$ and the pair distribution function $g(r)$:

$$F(r) = 4\pi r[\rho(r) - \rho_0] = \frac{2}{\pi}\int_0^{Q_{max}} Q(S(Q)-1)\sin(Qr)dQ \quad (2)$$

$$g(r) = \frac{\rho(r)}{\rho_0} \quad (3)$$

where $\rho(r)$ is the average atomic density, ρ_0 is the atomic density, r is the radial distance, Q is the scattering momentum and Q_{max} is the maximum scattering momentum up to which data have been collected, typically around 70–80 nm^{-1} in these DAC experiments.

As in a liquid metal, no atom is expected to sit at distances below than that of the 1st coordination shell, we can define a minimal distance r_{min} as (Fig. 2):

$$F(r) = -4\pi r\rho_0 \quad \text{for } 0 < r < r_{min} \quad (4)$$

This is the critical assumption in order to extract the density value. It is possible to show this assumption is fulfilled only for one specific density value (Eggert et al., 2002) (Fig. 2). An iterative procedure is performed to reduce oscillations in the low r region, due to small variations during the normalization procedure (Eggert et al., 2002; Kaplow et al., 1965). We can calculate the difference between model and data before the first iteration $\Delta F_0(r)$ such as:

$$\Delta F_0(r) = -F_0(r) - 4\pi r\rho_0 \quad (5)$$

We define a figure of merit to extract density ρ_0 and scaling factor b from the data analysis, as these values are independent from the iterative procedure:

$$\chi^2(\rho_0, b) = \int_0^{r_{min}} [\Delta F_i(r)]^2 dr \quad (6)$$

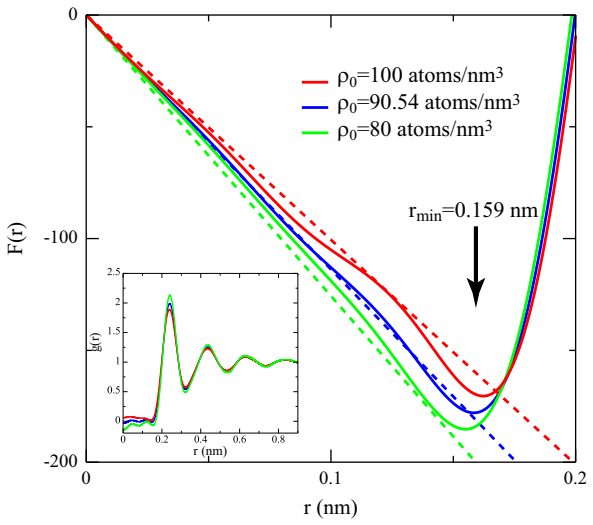

Fig. 2. Zoom on the low r region of the distribution function $F(r)$ (straight lines), calculated using different density values, and compared with the function $-4\pi r\rho_0$ (dashed lines) (Fe–Ni–S liquid at experimental conditions of 50 GPa and 2150 K). Differences between both functions are minimal for the right density value (90.54 atoms/nm^3) between 0 and r_{min} (Eq. (A18)). A clear deviation between $-4\pi r\rho_0$ and $F(r)$ could be observed for density of 80 and 100 atoms/nm^3. Value of the calculated minimal distance r_{min} is shown with an arrow. Inset: corresponding pair distribution functions $g(r)$. The correct $g(r)$ shows small oscillation around 0 in the small r region (blue curve). (For interpretation of the references to color in this figure legend, the reader is referred to the web version of this article.)

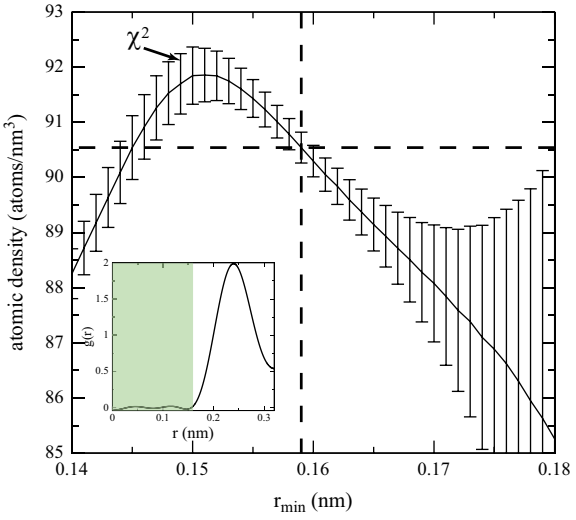

Fig. 3. Atomic densities calculated for different values of the minimal distance r_{min} (Fe–Ni–S liquid at experimental conditions of 50 GPa and 2150 K). Error bars show the value of the figure of merit χ^2 at each r_{min}. Orthogonal dashed lines point out the local minimum of the figure of merit, providing atomic density and r_{min} for this data set. Inset: Calculated $g(r)$ using previously determined parameters. Shaded area corresponds to the zone where the minimization was performed.

where $\Delta F_i(r)$ is the distribution function between 0 and r_{min} after "i" iterations. The value of χ^2 exhibits a well defined minimum close to 0, which gives the atomic density ρ_0 and the scale factor b for a given value of r_{min}. This last free parameter is adjusted by calculating χ^2 and finding a local minimum as a function of r_{min} (Fig. 3). The position of r_{min} corresponds to the base of the first coordinence sphere in the $g(r)$ (Fig. 3, inset).

Uncertainties affecting this process come from several factors. Firstly, the limited Q range resulting in loss of the information present at large Q affects the values of density determined using

the hereby procedure. This source of error is small however because the structure factor of liquid metals naturally damps with increasing Q, so that the main part of the information is comprised in the first two oscillations. Truncation effects, with a Q_{max} value of 70–80 nm^{-1} as in these experiments, are thus limited to ± 2.0 atoms/nm^3. This error bar is estimated from similar experiments on liquid iron alloys carried out using a Paris Edinburgh press that grants access to a wider Q range.

Secondly, atomic density extracted from diffraction patterns is very sensitive to r_{min}, as pointed out in Shen et al. (2004). The reliability of the obtained r_{min} can be judged by analysis of the pair correlation function. Indeed, for simple liquids, the value of this parameter should be close to the rise of the first coordinance sphere in $g(r)$. As shown in Fig. 3, the figure of merit χ^2, represented by the error bars on the curve, shows a local minimum around 0.159 nm. This analysis is performed in order to find r_{min} for spectrum. Variation of ± 0.01 nm on r_{min} leads to uncertainty of ~ 1 atoms/nm^3.

Summing up these two main sources of uncertainties, we estimate an error bar of ± 3 atoms/nm^3, corresponding to an uncertainty of ~ 250 kg/m^3 on density.

3. Results

Densities of Fe–5 wt% Ni–12 wt% S and Fe–5 wt% Ni–15 wt% Si liquid alloys were thus measured up to megabar conditions (Fig. 4) at temperatures between 2200 and 3000 K, and between 2500 and 3200 K, in Fe–Ni–S and Fe–Ni–Si alloys, respectively. Over this temperature range, density changes associated to the temperature variation are within the density error (see pure Fe EoS in Fig. 4), thus we decided to use the density at average temperature as normalized

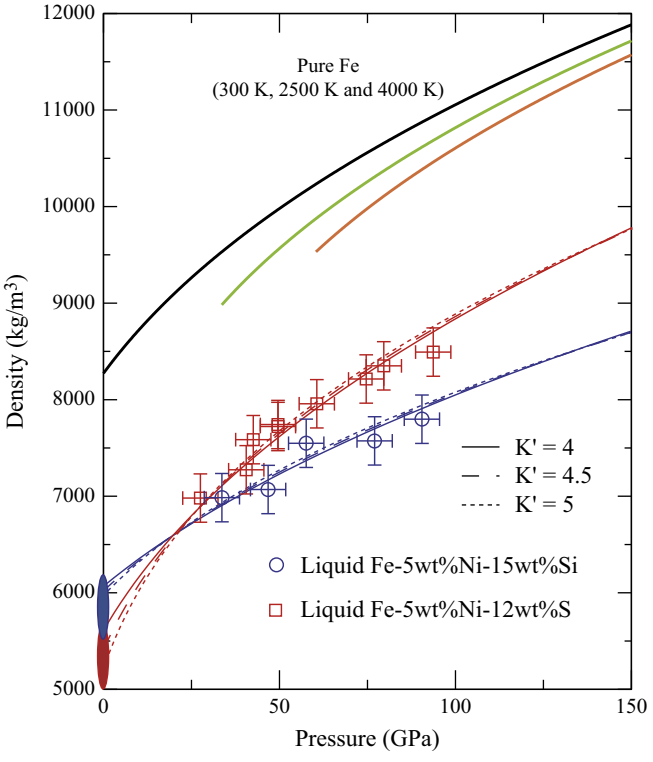

Fig. 4. Densities of liquid Fe-5 wt% Ni-12 wt% S and Fe-5 wt% Ni-15 wt% Si as a function of pressure. Lines (same code as in Fig. 5) are third order Birch–Murnaghan fits using different K' values (see text and Tables 1 and 2). These equations of state are in good agreement with density data at ambient pressure shown with their uncertainty ranges as two ellipses recalculated from Dumay and Cramb, (1995); Kress et al., (2008).

density (2600 K for Fe–Ni–S and 2850 K for Fe–Ni–Si). This assumption is based on the fact that the density changes associated to the maximal temperature variations in the present study are less than the experimental error bar of ± 250 kg/m^3 (for pure Fe, density variations associated with temperature variations of 800 K are 180 kg/m^3 at 50 GPa and 110 kg/m^3 at 100 GPa (Fiquet et al., 2007)). The back extrapolation of those measurements to ambient pressure is in good agreement with ambient pressure density measurements (Dumay and Cramb, 1995; Kress et al., 2008), corrected for thermal effects using thermal expansion of pure iron (Assael et al., 2006) (Fig. 4). We observe a density cross over between S- and Si-bearing compositions at around 25 GPa (Fig. 4). This implies that Si affects more the density of liquid Fe than S at pressures higher than 25 GPa and thus under Earth's core conditions. This observation contradicts the conclusion reached in previous works (Poirier, 1994) based on 1 bar measurements, but is in good agreement with *ab initio* calculations (Alfè et al., 2002). The effect of Si on density measured in the present study is stronger than that observed in early shock measurements (8700 kg/m^3 for 15 wt% Si compared to ~ 10000 kg/m^3 for 20 wt% Si at a pressure of 150 GPa (Balchan and Cowan, 1966)). Further discussion of the exact conditions reached in those dynamic compression experiments would be necessary to understand this discrepancy (Luo and Ahrens, 2004).

The experimental data can then be used to fit analytical equations of state (EoS) of the two liquids. Instead of using the pressure density data given in Fig. 4 which could be retrieved for a limited number of data points only, we decided to use the position of the first diffuse peak in the liquid diffraction signal (d) which allowed considering more data points (see Appendix B). Indeed, only few selected high-quality diffraction patterns were processed for retrieving density data, whereas d positions were measured in more than five patterns at each pressure step, by Gaussian fit to the diffuse main peak. As a matter of fact, it has been shown, in the case of metallic amorphous compounds, that the specific volume is proportional to d^3 (Jiang et al., 2004). This linear relation is particularly true when the structure of the liquid is compact and when the number of atoms sitting in the first coordination shell remains constant under compression (see CN1 in Table 1). Therefore, we used the fictive volume d^3 as a proxy for the specific volume, with the advantage of having more data available and thus ultimately more reliable estimations of the isothermal bulk modulus $K_{T,0}$ and of its first pressure derivative K' (Fig. 5).

The d^3 values have been fit for both alloys (Table 2) using a third order Birch–Murnaghan equation of state:

$$f = \frac{\rho}{\rho_A} = \frac{V_A}{V} = \frac{d_A^3}{d^3} \tag{7}$$

$$P = \frac{3K_{T,0}}{2}(f^{7/3} - f^{5/3})\left[1 + \frac{3}{4}(K' - 4)(f^{2/3} - 1)\right] \tag{8}$$

$$K_T = \frac{K_{T,0}}{2}\left[(7f^{7/3} - 5f^{5/3})\left(1 + \left(\frac{3}{4}(K' - 4)(f^{2/3} - 1)\right)\right) + \left(\frac{3}{4}K_{T,0}(K' - 4)(f^3 - f^{7/3})\right)\right] \tag{9}$$

In Eq. (7), the indices A refer to ambient pressure. The data set remains insufficient to perform an accurate inversion of unique values of room pressure volume V_A, bulk modulus ($K_{0,T}$) at $P = P_0 = 1$ bar and of its first pressure derivative (K'). We decided to fix K' values at different plausible values (4.0, 4.5, 5.0). Then, at each fixed K' value, fit of d^3 data provided $K_{T,0}$ and ${d_A}^3$ (fictive volume at ambient pressure) values (Table 2 and Fig. 5). Then, values of ρ_A (density at ambient pressure) were obtained for each couple of values of K' and $K_{T,0}$ by calculating scaling factors between d^3 and actual volumes in those cases where density values derived for selected high quality spectra were available (Table 1). Measured densities were converted in volume and

Table 1
Physical and structural properties of liquid iron alloys. Error bars are in brackets. CN1 and CS1 are respectively the coordination number and the position of the first coordinence sphere measured on the $g(r)$.

	P (GPa)	T (K)	r_{min} (nm)	b	ρ_0 (atoms/nm^3)	χ^2	Density (kg/m^3)	Max CS1 (nm)	CN1 (atoms)
Fe–5 wt%Ni–12 wt%S									
FeNiS4_40	28 (5)	2370 (150)	0.154	0.978	81.86	0.008	6978 (250)	0.251	9.12
FeNiS1_65	41 (5)	2140 (150)	0.163	0.979	85.29	0.223	7270 (250)	0.246	9.14
FeNiS4_73	43 (5)	2460 (150)	0.161	0.966	88.95	0.26	7582 (250)	0.244	9.47
FeNiS1_26	50 (5)	2150 (150)	0.159	0.96	90.54	0.28	7717 (250)	0.242	9.27
FeNiS1_28	50 (5)	2330 (150)	0.158	0.958	90.78	0.257	7738 (250)	0.241	9.15
FeNiS4_110	61 (5)	2490 (150)	0.162	0.972	93.3	0.5	7953 (250)	0.241	9.48
FeNiS2_40	75 (5)	2650 (150)	0.159	0.978	96.31	0.498	8209 (250)	0.237	9.14
FeNiSNico_30	80 (5)	2830 (150)	0.156	0.973	97.9	0.117	8345 (250)	0.239	9.77
FeNiS2_85	94 (5)	2750 (150)	0.155	0.958	99.57	0.371	8487 (250)	0.234	8.83
Fe–5 wt%Ni–15 wt%Si									
FeNiSi3_22	34 (5)	2520 (150)	0.164	0.97	86.46	0.288	6982 (250)	0.258	9.58
FeNiSi1_20	47 (5)	2790 (150)	0.16	0.972	87.38	0.084	7057 (250)	0.247	9.47
FeNiSi3_85	58 (5)	3220 (150)	0.158	0.982	93.42	0.158	7544 (250)	0.244	9.83
FeNiSi6_38	77 (5)	3000 (150)	0.16	0.991	93.73	0.251	7569 (250)	0.243	9.9
FeNiSi6_105	91 (5)	3200 (150)	0.154	0.965	96.5	0.792	7793 (250)	0.238	9.05

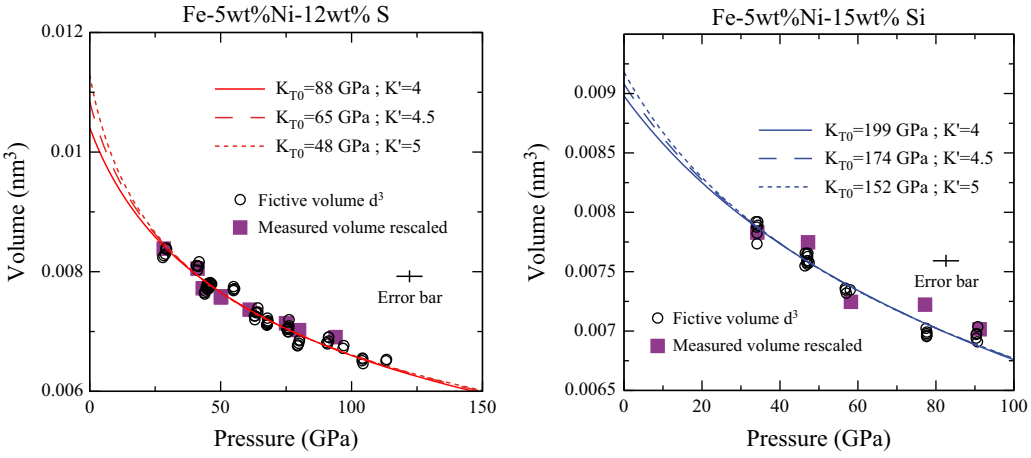

Fig. 5. Fictive volume d^3, obtain from the position of the diffuse broad signal of the liquid d, as a function of pressure for Fe-5 wt%Ni-12 wt% S and Fe-5 wt%Ni-15 wt% Si liquid alloys. These fictive volumes are compared with density values measured here, rescaled by comparison between ambient pressure fictive volume and ambient pressure density value. Lines are third order Birch–Murnaghan fits using different K′ values (see text and Tables 1 and 2).

Table 2
Third order Birch–Murnaghan fit parameters for the liquid iron alloys at temperatures of 2600 K for Fe–Ni–S and 2850 K for Fe–Ni–Si.

	$K'=4$	$K'=4.5$	$K'=5$
Fe–5 wt% Ni–12 wt% S			
K_0 (GPa)	88 ± 7	65 ± 6	48 ± 6
$d_A{}^3$ (Å^3)	10.4 ± 0.2	10.8 ± 0.2	11.3 ± 0.3
ρ_A (kg/m^3)	5600 ± 100	5400 ± 100	5200 ± 100
Fe–5 wt% Ni–15 wt% Si			
K_0 (GPa)	199 ± 16	174 ± 16	153 ± 15
$d_A{}^3$ (Å^3)	9 ± 0.1	9.1 ± 0.1	9.2 ± 0.1
ρ_A (kg/m^3)	6050 ± 100	6000 ± 100	5950 ± 100

rescaled using ratio between $d_A{}^3$ and ρ_A. Good agreement is found between these fictive volumes and measured volumes (Fig. 5), strengthening the validity of our EoS determination method. As already mentioned, the calculated values of ρ_A found here are in good agreement with ambient pressure densities recalculated from (Dumay and Cramb, 1995; Kress et al., 2008) for average temperatures of 2600 K for Fe–S alloys and 2850 K for Fe–Si alloys using thermal expansion of liquid iron (Assael et al., 2006). A brief estimation of the role of the 5 wt% of Ni shows that the effect on density is insignificant. As 5 wt% Ni do not significantly affect elastic properties of the alloy (Antonangeli et al., 2010; Komabayashi et al., 2012), a simple calculation of specific masses leads to density variations of less than 0.2% when Ni-bearing and Ni-free compositions are compared.

Isothermal EoS of density and bulk modulus of the two alloys (at 2600 K for Fe–Ni–S and 2850 K for Fe–Ni–Si) are shown in Fig. 6. For comparison of the bulk moduli between geophysical data and experimental values, it was necessary to calculate the isothermal K_T from the adiabatic K_S provided by the PREM model (Dziewonski and Anderson, 1981) using temperature and thermal parameters of the Earth's core (Brown and Shankland, 1981) (Fig. 6). The densities and isothermal bulk moduli of the S and Si bearing alloys were also compared with those of solid Fe at 300 K and at 4000 K (Fiquet et al., 2007). We note that the density and compressibility differences between liquid and solid Fe under Earth's core conditions (estimated at around 2% (Alfè et al., 2002)) are less than the error bar on the measurements (5–6%) (Fig. 6).

4. Discussion

Direct comparison between PREM model and equation of state of Fe liquid alloys (Fig. 6) shows that S as the only light element in

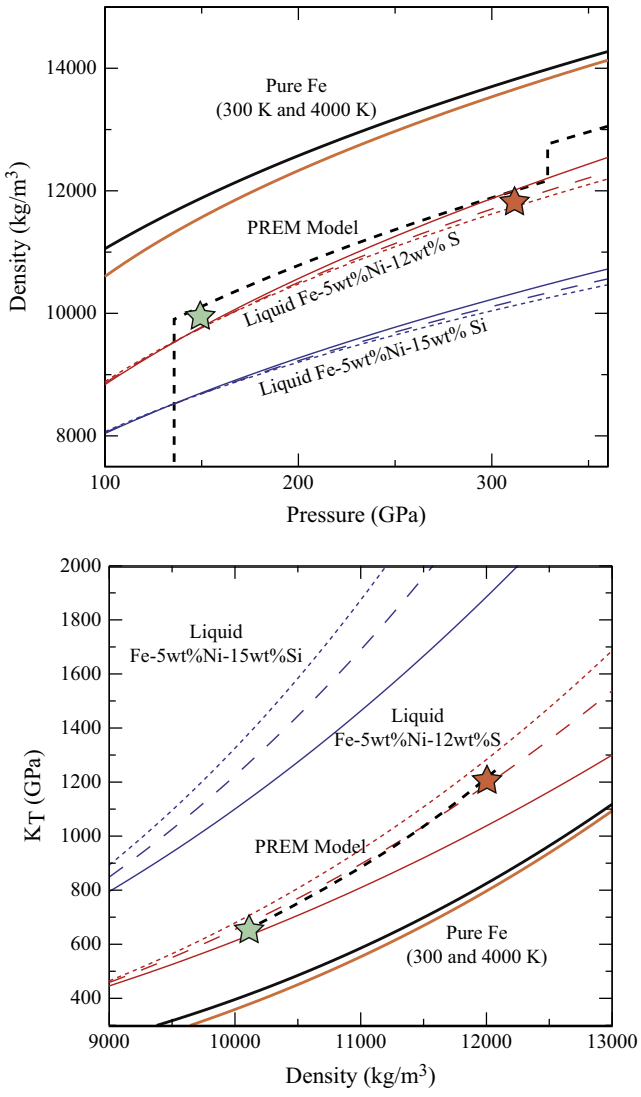

Fig. 6. Density and isothermal bulk modulus (K_T) of Fe–5 wt% Ni–12 wt% S and Fe–5 wt% Ni–15 wt% Si liquid alloys at average temperatures (2600 K for Fe–Ni–S and 2850 K for Fe–Ni–Si alloys) compared with solid iron (Fiquet et al., 2007) and PREM model (dashed line) (Dziewonski and Anderson, 1981). In the case of PREM, adiabatic bulk modulus has been converted to isothermal bulk modulus (see text). Stars corresponds to the central solution calculated using the linear interpolations (see text).

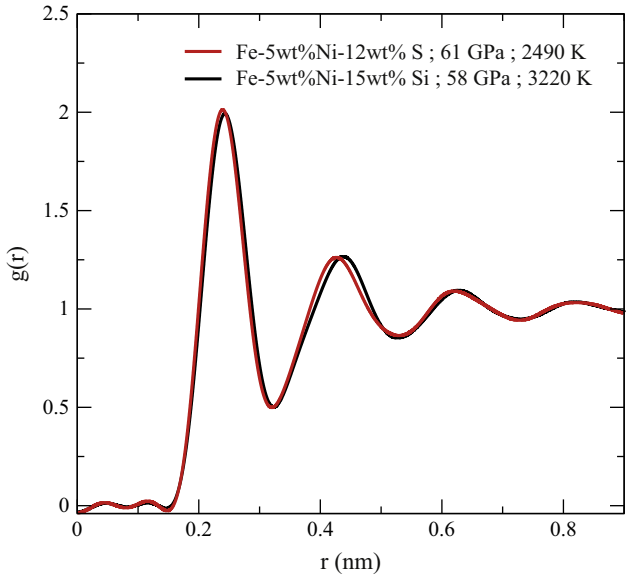

Fig. 7. Pair distribution function $g(r)$ of the Fe alloys at similar pressure conditions.

Table 3
Parameters and corresponding uncertainities (Δ) used for the envelope of solutions determination in Fig. 7. Densities in parenthesis correspond to value calculated from the EoS at the average temperatures (2600 K for Fe–S alloys and 2850 K for Fe–Si alloys). The density values without parentheses are corrected for thermal effects (to temperatures of 4000 K at 150 GPa and 6500 K at 312 GPa).

150 GPa	K_T (GPa)	Δ	Density (kg/m^3)	Δ
150 GPa				
Fe	376	25	11,580	50
Fe–15 wt% Si	1262	100	8230 (8410)	250
Fe–12 wt% S	679	50	9590 (9765)	250
PREM	653	10	10,110	25
312 GPa				
Fe	782	70	13,560	300
Fe–15 wt% Si	2250	300	9870 (10,200)	500
Fe–12 wt% S	1190	100	11,530 (11820)	500
PREM	1216	10	12,000	50

the Earth's core is compatible with seismological data, for content of 12 wt% S. On the other hand, 15 wt% Si is too high to fit with the PREM model. Furthermore, strong divergence under high pressure between compressibility of this Fe-15 wt% Si liquid alloy shows that Si could not be present in large amount in the Earth's core. Similarities of the liquid alloys structures at 50 GPa (Fig. 7) are in agreement with previous publications, showing that S does not disturb the liquid long-range order at pressure over 15 GPa (Morard et al., 2007, 2008a, 2008b). So it seems difficult to simply explain the difference in compressibility from a structural point of view. However, it would be necessary to have more detailed structural information on the liquid alloys, using different experimental techniques, to conclude on this point.

Two linear interpolations are used to estimate S and Si content in the Earth's liquid outer core from the experimental results described above:

$$\rho_{PREM} = \rho_{Fe}(1-X_S-X_{Si}) + \rho_{Si}X_{Si} + \rho_S X_S \quad (10)$$

$$K_{T,PREM} = K_{T,Fe}(1-X_S-X_{Si}) + K_{T,Si}X_{Si} + K_{T,S}X_S \quad (11)$$

Theoretically, Eqs. (10) and (11) are mutually inconsistent. However, taking into account the experimental precision of the present study and the small S or Si content (0–15 wt%), this linear approximation is the most reasonable method for using the available data while involving a minimal number of parameters. It is supported by low pressure density measurements (Nishida et al., 2008; Tateyama et al., 2011) and by sound velocity determinations (Badro et al., 2007; Antonangeli et al., 2010). Eqs. (10) and (11) imply the following parameters (Table 3): ρ_{Fe} and $K_{T,Fe}$ taken from Fiquet et al. (2007), ρ_{Si}, $K_{T,Si}$, ρ_S, $K_{T,S}$, obtained by linear interpolation between pure Fe data and the parameters of the two alloys given in Table 3, and finally ρ_{PREM} and $K_{T,PREM}$. From this, the weight fractions of Si and S in the Earth's outer core, X_{Si} and X_S can be deduced.

The densities of the two liquid alloys are corrected for differences of temperature between the measured isothermal EoS (2600 K for Fe–Ni–S and 2850 K for Fe–Ni–Si) and the Earth's core (4000 K at 150 GPa and 6500 K at 312 GPa, (Morard et al., 2011)) (Table 3). This correction follows the assumption of constant $\alpha_0 \times K_{T,0}$ from ambient up to the Earth's inner core pressure. In order to perform this correction, we used thermal expansion α_0 of pure liquid iron at ambient pressure, measured between 1800 K and 2500 K (Assael et al., 2006) and $K_{T,0}$ from the experimental EoS.

Hence, the thermal expansions of the alloys under high pressure and temperature $\alpha_{P,T}$, were recalculated and thus the densities of the two alloys at 4000 K, 150 GPa and 6500 K, 312 GPa (Morard et al., 2011) (Table 3).

In order to determine the domain of solutions of the coupled Eqs. (10) and (11), we performed a random draw of parameter values within their error bars (Table 3). The error bars on the density measurements were discussed previously. Error bars on bulk modulus are derived from the uncertainties on density data and from the dispersion induced by the different values of K' tested. Uncertainties on the PREM model and on experimental Fe data were taken from the literature (Dziewonski and Anderson, 1981; Fiquet et al., 2007). The pressures chosen for comparison with our calculated EoS are shifted from the CMB and IOCB (150 GPa instead of 135 GPa; 312 GPa instead of 335 GPa) in order to avoid any problems of chemical heterogeneity and disagreement between different radial seismological models concerning these boundary layers. The uncertainties on these values were propagated using Monte Carlo simulations (Siebert et al., 2011) and allowed to draw envelopes of possible compositions of Fe–Si–S alloys matching Earth's core values at the two selected pressures, 150 GPa and 312 GPa (Fig. 8). At the pressure of 150 GPa, which does not require large extrapolations away from the experiments, the central solution (exact solution of the coupled Eqs. (10) and (11)) is at 2.0 wt% of Si and 5.9 wt% of S (Fig. 8). The same calculation performed at 312 GPa yielded a central solution at 2.3 wt% of Si and 5.5 wt% of S. The same composition should fit the entire outer core which is likely to be chemically homogeneous (Souriau et al., 2003). Therefore, taking in account the error bars, a composition of 2 wt% of Si and 6 wt% of S provides the best agreement of the measurements with the PREM model (Fig. 8).

The model results at 150 GPa (Fig. 8) exclude Si as the only light element in the Earth's outer core. Moreover, the presence of large amounts of Si is unlikely due to the divergence between the isothermal bulk modulus of Fe–Ni–Si alloys and the PREM model (Fig. 6B). A similar conclusion has been reached in solid Fe–Si alloys, suggesting 1–2 wt% Si as the maximum Si content in the Earth's inner core (Antonangeli et al., 2010). Provided a solid solution behavior in the Fe–FeSi system under core conditions (Alfè et al., 2002; Kuwayama et al., 2009), partitioning values between liquid and solid should be close to 1, implying that Si contents superior to 3–4 wt% are very unlikely in the Earth's outer core. This is in slight disagreement with a majority of geochemical models for Earth's core composition (Allègre et al., 1995; McDonough, 2003).

In contrast, the elastic properties of the sulfur-bearing liquid Fe-alloy are well consistent with the geophysical data. The model results (Fig. 8) even admit sulfur as the only light element in the Earth's liquid core (~10 wt% S). The central solution, an Earth's core with 6 wt% S, however appears contradictory with most bulk Earth geochemical models (Allègre et al., 1995; Dreibus and Palme, 1995) even though some of the possible solutions shown in Fig. 8 might still be marginally consistent with those geochemical models: for example, a S-content bracketed between 1.5 and 2.5 wt% S and an Si content between 4 and 5 wt% would agree with Allègre et al. (1995) and Dreibus and Palme (1995). We stress, however, that these values are at the extreme limit of the model domain (Fig. 8), and still in disagreement with conclusions derived from sound velocities measurements previously mentioned (Antonangeli et al., 2010).

The effect of O on the EoS of liquid iron has yet to be measured at relevant pressure and temperature conditions. Recent shock and static compression experiments are not in favor of O as a major light element in the Earth's core (Huang et al., 2011; Sata et al., 2010) in spite of its affinity with the metallic phase during Earth's differentiation (Siebert et al., 2012). Classically, oxygen contribution to the density jump at IOCB is considered dominant, because it is expected to remain extremely incompatible with the liquid outer core (estimation from *ab initio* calculations of density jump at IOCB suggests a maximum of 2.5 wt% O in the liquid outer core (Alfè et al., 2002)), whereas Si and S would induce a much smaller density contrast. However, the situation is not so clear as recent studies suggest that S solubility in solid Fe remains rather low even at core pressures (Kamada et al., 2010; Li et al., 2001). Therefore, S could also potentially explain the density jump at IOCB.

Usually, disregard of S as an important element of the Earth's core comes from the low temperature of condensation of sulfur which should have led to strong depletion of this element in the bulk Earth, at least to an extent similar to the well reported depletions of some lithophile volatile elements (Dreibus and Palme, 1995). We notice however that specific atypic nebular environments could still retain some sulfur because of particular chemical bounds such as FeS or SiS (Pasek et al., 2005). Moreover and more likely, during Earth accretion, some S-rich cores of planetary building blocks of the Earth may have joined its growing core without having enough time for losing all their sulfur (Rudge et al., 2010).

5. Summary

Density measurements of liquid Fe–5 wt% Ni–12 wt%S and Fe–5 wt% Ni–15 wt% Si alloys under high pressure and temperature

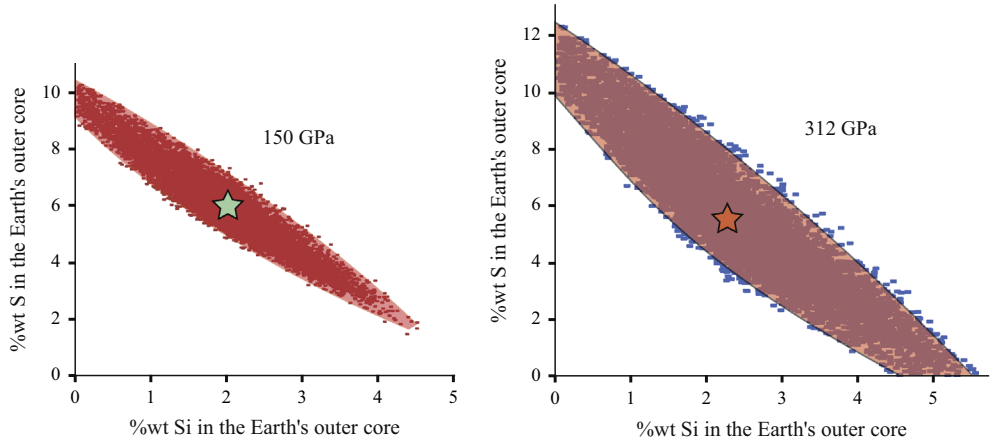

Fig. 8. Envelopes representing the solution domains for S and Si contents in the Earth's core at 150 GPa and 312 GPa, simultaneously matching both density and K_T from PREM model. Central solutions are represented with stars.

have been performed by *in situ* X-ray diffraction in laser-heated diamond anvil cells. These data have been fitted using third order Birch–Murnaghan equations of state and extrapolated up to Earth's outer core conditions, highlighting that Si has a stronger effect than S on density and compressibility of liquid iron. Using a simple linear mixing model for density and compressibility, an Earth's outer core composition with 6% of sulfur and 2% of silicon by weight is found to best explain its geophysical signature, although in contradiction with geochemical models assuming strong volatilization of sulfur during Earth's formation.

Acknowledgments

The authors thank the ESRF staff of the High Pressure Beamline ID27 (S. Bauchau and M. Mezouar) for the X-ray experiments, and P. Ochin (Institut de Chimie et des Matériaux de Paris-Est, Paris, France) for the starting materials synthesis. We also thank G. Fiquet and J. Badro for fruitful discussions. This work was supported by the French National Research Agency (ANR) Grant no. 2010-JCJC-604-01 and the PlanetLab program of French National Research Agency (ANR) Grant no. ANR-12-BS04-0015-04. The original manuscript was improved by the constructive comments of J. Wade and two anonymous reviewers.

Appendix A. Analysis of diffuse signal from liquids

A. Theoretical background

For a polyatomic compound, the spherically averaged coherent X-ray scattering from N disordered atoms is written as:

$$I_{coh}(Q) = N\sum_p f_p^2(Q) + \sum_m^{m\neq n}\sum_n^{n\neq m} f_m f_n \frac{\sin(Qr_{mn})}{Qr_{mn}} \tag{A1}$$

where m, n are the atomic species in the sample, f_i is the atomic form factor and $Q=(4\pi\sin\theta)/\lambda$ is the scattering momentum. The first summation is done for the atoms composing an elementary unit (smallest chemical unit), the second one is done for all the atom pairs in the sample. The convention, as used in Eggert et al. (2002), is that m and n define atoms in the entire volume, and p and q define atoms in the elementary unit. In this way, we can define the average atomic density $\rho_{p,q}(r)$ such as:

$$\rho_{p,q}(r)dV = \langle \rho_p(r_{p,q})dV_q \rangle \tag{A2}$$

which represents the number of type q atoms in an elementary volume dV at a distance r of a type p atom. Then, Eq. (A1) is rearranged as:

$$I_{coh}(Q) = N\sum_p f_p^2(Q) + N\sum_p\sum_q \int_S f_p(Q)f_q(Q)\rho_{p,q}(r)\frac{\sin Qr}{Qr}dV \tag{A3}$$

Contrary to the definition of the structure factor in Eggert et al. (2002) who used the Ashcroft–Langreth method (Ashcroft and Langreth, 1966), we prefer to use the Faber–Ziman method (Faber and Ziman, 1965). The advantage of this definition is that the structure factor is normalized to unity, enabling direct comparison between samples with different compositions (Morard et al., 2007). In that case, we need to define the following functions:

$$\frac{1}{N}\sum_p f_p^2(Q) = \sum_i X_i f_i^2(Q) = \langle f^2 \rangle \tag{A4}$$

$$\frac{1}{N}\sum_p\sum_q f_p(Q)f_q(Q) = \sum_i\sum_j X_i f_i(Q) X_j f_j(Q) = \langle f \rangle^2 \tag{A5}$$

$$\rho(r) = \sum_p\sum_q X_p X_q f_p(Q) f_q(Q)\rho_{pq}(r)/\langle f \rangle^2 \tag{A6}$$

Then the Eq. (A3) becomes:

$$I_{coh}(Q) = \langle f^2 \rangle + \langle f \rangle^2 \int_0^\infty 4\pi r^2 \left[\rho(r)-\rho_0\right]\frac{\sin Qr}{Qr}dr \tag{A7}$$

where ρ_0 is the atomic density of the studied material.

The Faber–Ziman structure factor $S_{FZ}(Q)$ is defined as follows (Waseda, 1980):

$$S_{FZ}(Q) = \frac{[I_{coh}(Q)-(\langle f^2 \rangle - \langle f \rangle^2)]}{\langle f \rangle^2} = 1 + \int_0^\infty 4\pi r^2 \left[\rho(r)-\rho_0\right]\frac{\sin Qr}{Qr}dr \tag{A8}$$

By Fourier transform of Eq. (A8), one obtains the distribution function $F(r)$ and the pair distribution function $g(r)$:

$$F(r) = 4\pi r\left[\rho(r)-\rho_0\right] = \frac{2}{\pi}\int_0^{Q_{max}} Q(S_{FZ}(Q)-1)\sin(Qr)dQ \tag{A9}$$

$$g(r) = \frac{\rho(r)}{\rho_0} \tag{A10}$$

A.2. Krogh-Moe–Norman normalization

The scattering signal from the sample $I_S(Q)$ is extracted from the measured signal $I_{meas}(Q)$ as follows:

$$I_S(Q) = I_{meas}(Q) - bI_{bk}(Q) \tag{A11}$$

where $I_{bk}(Q)$ is the background signal coming from the environment of the sample (mostly Compton signal from the diamonds, in the case of diamond-anvil-cell experiments). This signal is usually acquired under very close pressure–temperature conditions but without scattering from the melt (i.e. at sufficiently lower temperature to suppress melt) and adjusted by a scale factor b to account for the slight difference in experimental conditions.

Following the method developed by Krogh-Moe (Krogh-Moe, 1956) and Norman (Norman, 1957), $I_S(Q)$ is converted into the normalized structure factor units:

$$S_{FZ}(Q) = \frac{I_{coh}(Q)-(\langle f^2 \rangle - \langle f \rangle^2)}{\langle f \rangle^2} = \frac{[\alpha_{FZ} I_S(Q) - \sum I_{Incoh}(Q)] - (\langle f^2 \rangle - \langle f \rangle^2)}{\langle f \rangle^2} \tag{A12}$$

$$\alpha_{FZ} = \frac{-2\pi^2\rho_0 + \int_0^{Q_{max}}(\sum I_{Incoh}(Q) + \langle f^2 \rangle/\langle f \rangle^2)Q^2 dQ}{\int_0^{Q_{max}}(Q^2 I_S(Q)/\langle f \rangle^2)dQ} \tag{A13}$$

where Q_{max} is the maximum scattering momentum, typically around 70–80 nm^{-1} for DAC experiments, and $\sum I_{Incoh}(Q)$ is the sum of the incoherent scattering signals from the sample. The effect of the limited Q range, in particular on the density, will be discussed later. Note that the Q range used in the present study is suitable for the study of amorphous or liquid compounds (Clayton and Heaton, 1961) and does not lead to spurious peaks in the $g(r)$ (Waseda, 1980).

A.3. Iterative procedure

The iterative procedure presented here shows some differences with Eggert et al. (2002) due to the specificities of liquid metals. Firstly, we did not take into account possible errors in the molecular form factor. In metallic alloys without strong molecular bonds, this error can be neglected. Secondly, we did not take into account intramolecular contributions to the distribution function, because such contributions do not exist in the studied disordered metals.

This procedure, following the work of Kaplow et al. (1965), states that small variations of the normalization factor α_{FZ} could lead to large variations in $g(r)$. These variations are noted as $\Delta\alpha_{FZ}$ and $\Delta i(Q)$.

We define:

$$i(Q) = S_{FZ}(Q) - 1 \tag{A14}$$

$$i(Q) = i_0(Q) + \Delta i(Q) \tag{A15}$$

$$\alpha_{FZ} = \alpha_{FZ}(1 + \Delta\alpha_{FZ}) \tag{A16}$$

where

Then, we write:

$$Q\Delta i(Q) = Q\Delta\alpha_{FZ}S_0(Q) = \Delta\alpha_{FZ}[Qi_0(Q) + Q] = \Delta\alpha_{FZ}Qi_0(Q) + \Delta\alpha_{FZ}Q \tag{A17}$$

where index 0 represents the value of the function before the first iteration. Expression (A17) contains two terms: the first one is a scaling factor for $S(Q)$, and the second one, called ramp term, leading to large oscillation in the low r region of the $g(r)$ (Eggert et al., 2002).

In the distribution function $F(r)$, one can define a minimal distance r_{min} such as the distance between 0 and r_{min} represents the largest distance where no atom can be found. One therefore obtains

$$F(r) = -4\pi r\rho_0 \quad \text{for } 0 < r < r_{min} \tag{A18}$$

This is the basic assumption in order to extract the density value of material. One can show that this is true only for one exact density value (Eggert et al., 2002) (Fig. 3). Then, one can calculate the difference between model and real data before the first iteration $\Delta F_0(r)$ such as:

$$\Delta F_0(r) = -F_0(r) - 4\pi r\rho_0 \tag{A19}$$

Assessing that perturbation signal mainly comes from the ramp term in Eq. (A17), one can define the following Fourier transform of Eq. (A19):

$$\Delta\alpha Q = \int_0^{r_{min}} \Delta F_0(r)\sin(Qr)dr \tag{A20}$$

Finally, one can calculate an ameliorated structure factor (first step of the iteration) by subtracting the variation term to the 0 iteration step $\Delta i_0(Q)$ using Eqs. (A17) and A20):

$$\begin{aligned} i_1(Q) &= i_0(Q) - \Delta i_0(Q) = i_0(Q) - \Delta\alpha_0 S_0(Q) \\ &\Leftrightarrow = i_0(Q) - \frac{1}{Q}[\Delta\alpha Q i_0(Q) + \Delta\alpha Q] = i_0(Q) - \frac{1}{Q}[\Delta\alpha Q(i_0(Q) + 1)] \\ &\Leftrightarrow = i_0(Q) - \frac{1}{Q}(i_0(Q) + 1)\int_0^{r_{min}} \Delta F_0(r)\sin(Qr)dr \end{aligned} \tag{A21}$$

To express this directly in terms of structure factor, one writes:

$$S_1(Q) = S_0(Q)\left[1 - \frac{1}{Q}\int_0^{r_{min}} \Delta F_0(r)\sin(Qr)dr\right] \tag{A22}$$

This iterative procedure is generalized as follows:

$$(a)\ F_i(r) = \frac{2}{\pi}\int_0^{Q_{max}} Q(S(Q) - 1)\sin(Qr)dQ \tag{A23}$$

$$(b)\ \Delta F_i(r) = F_i(r) + 4\pi r\rho_0 \tag{A24}$$

$$(c)\ S_{i+1}(Q) = S_i(Q)\left[1 - \frac{1}{Q}\int_0^{r_{min}} \Delta F_i(r)\sin(Qr)dr\right] \tag{A25}$$

The convergence of this procedure is quite fast, usually after 3 iterations. One usually uses 5 steps, in order to verify convergence. This technique allows the reduction of oscillations at small r in $g(r)$. The atomic density is thus extracted from the diffuse scattering signal.

A.4. Density calculation

As shown in Eggert et al. (2002), it is possible to use a figure of merit to extract density ρ_0 and scaling factor b from the diffraction data analysis, as these values are independent from the iterative procedure:

$$\chi^2(\rho_0, b) = \int_0^{r_{min}} [\Delta F_i(r)]^2 dr \tag{A26}$$

This function exhibits one well defined minimum (Eggert et al., 2002). We used a minimization procedure (SIMPLEX method, (Nelder and Mead, 1965)) to find ρ_0 and b.

Appendix B. Supplementary material

Supplementary data associated with this article can be found in the online version at http://dx.doi.org/10.1016/j.epsl.2013.04.040.

References

Alfè, D., Gillan, M.J., Price, G.D., 2002. Composition and temperature of the Earth's core constrained by combining ab initio calculations and seismic data. Earth Planet. Sci. Lett. 195, 91–98.

Allègre, C.J., Poirier, J.P., Humler, E., Hofmann, A.W., 1995. The chemical composition of the Earth. Earth Planet. Sci. Lett. 134, 515–526.

Andrault, D., Fiquet, G., Itié, J.P., Richet, P., Gillet, P., Häusermann, D., Hanfland, H., 1998. Thermal pressure in the laser heated diamond anvil cell: an X-ray diffraction study. Eur. J. Mineral. 10, 931–940.

Antonangeli, D., Siebert, J., Badro, J., Farber, D.L., Fiquet, G., Morard, G., Ryerson, F.J., 2010. Composition of the Earth's inner core from high-pressure sound velocity measurements in Fe–Ni–Si alloys. Earth Planet. Sci. Lett. 295, 292–296.

Ashcroft, N.W., Langreth, D.C., 1966. Structure of binary liquid mixture. IPhys. Rev. 156, 685–692.

Assael, M.J., Kakosimos, K., Banish, R.M., Brillo, J., Egry, I., Brooks, R., Quested, P.N., Mills, K.C., Nagashima, A., Sato, Y., Wakeham, W.A., 2006. Reference data for the density and viscosity of liquid aluminum and liquid iron. J.Phys. Chem. Ref. Data 35, 285–300.

Aubert, J., Amit, H., Hulot, G., Olson, P., 2008. Thermochemical flows couple the Earth's inner core growth to mantle heterogeneity. Nature 454, 758–761.

Badro, J., Fiquet, G., Guyot, F., Gregoryanz, E., Occelli, F., Antonangeli, D., D'Astuto, M., 2007. Effect of light elements on the sound velocities in solid iron: implications for the composition of Earth's core. Earth Planet. Sci. Lett. 254, 233–238.

Balchan, A.S., Cowan, G.R., 1966. Shock compression of two iron–silicon alloys to 2.7 megabars. J. Geophys. Res. 71, 3577–3588.

Balog, P.S., Secco, R.A., Rubie, D.C., Frost, D.J., 2003. Equation of state of liquid Fe–10%wt S: implications for the metallic cores of planetary bodies. J. Geophys. Res. 108, 2124.

Birch, F., 1964. Density and composition of the mantle and core. J. Geophys. Res. 69, 4377–4388.

Boehler, R., De Hantsetters, K., 2004. New anvils design in diamond-cells. High Pressure Res. 24, 391–394.

Brown, J.M., Shankland, T.J., 1981. Thermodynamic parameters in the Earth as determined from seismic profiles. Geophys. J. R. Astron. Soc. 66, 579–596.

Chabot, N.L., 2004. Sulfur contents of the parental metallic cores of magmatic iron meteorites. Geochim. Cosmochim. Acta 68, 3607–3618.

Clayton, G.T., Heaton, L., 1961. Neutron diffraction study of krypton in the liquid state. Phys. Rev. 121, 649–653.

Corgne, A., Siebert, J., Badro, J., 2009. Oxygen as a light element: a solution to single-stage core formation. Earth Planet. Sci. Lett. 288, 108–114.

Dreibus, G., Palme, H., 1995. Cosmochemical constraints on the sulfur content in the Earth's core. Geochim. Cosmochim. Acta 60, 1125–1130.

Dumay, C., Cramb, A.W., 1995. Density and interfacial tension of liquid Fe–Si alloy. Metall. Mater. Trans. B 26B, 173–176.

Dziewonski, A.M., Anderson, D.L., 1981. Preliminary reference earth model. Phys. Earth Planet. Inter. 25, 297–356.

Eggert, J.H., Weck, G., Loubeyre, P., Mezouar, M., 2002. Quantitative structure factor and density measurements of high-pressure fluids in diamond anvil cells by X-ray diffraction: argon and water. Phys. Rev. B 65, 174105.

Faber, T.E., Ziman, J.M., 1965. A theory of electrical properties of liquid metals. 3. Resistivity of binary alloys. Philos. Mag. 11, 153.

Fiquet, G., Badro, J., Auzende, A., Gregoryanz, E., Siebert, J., Matas, J., Guignot, N., 2007. A new thermal equation of state for iron at megabar pressure. EoS Trans. AGU 88 DI24A-05.

Huang, H., Fei, Y., Cai, L., Jing, F., Hu, X., Xie, H., Zhang, L., Gong, Z., 2011. Evidence for an oxygen-depleted liquid outer core of the Earth. Nature 479, 513–517.

Jiang, J.Z., Rozeker, W., Sikorski, M., Cao, Q.P., Xu, F., 2004. Pressure effect of glass transition temperature in Zr46.8Ti8.2Cu7.5Ni10Be27.5 bulk metallic glass. App. Phys. Lett. 84, 1871–1873.

Kamada, S., Terasaki, H., Ohtani, E., Sakai, T., Kikegawa, T., Ohishi, Y., Hirao, N., Sata, N., Kondo, T., 2010. Phase relationships of the Fe–FeS system in conditions up to the Earth's outer core. Earth Planet. Sci. Lett. 294, 94–100.

Kaplow, R., Strong, S.L., Averbach, B.L., 1965. Radial density function for liquid mercury and lead. Phys. Rev. 138, 1336–1345.

Komabayashi, T., Hirose, K., Ohishi, Y., 2012. In situ X-ray diffraction measurements of the fcc–hcp phase transition boundary of an Fe–Ni alloy in an internally heated diamond anvil cell. Phys. Chem. Miner. 39, 329–338.
Kress, V., Greene, L.E., Ortiz, M.D., Mioduszewski, L., 2008. Thermochemistry of sulfide liquids IV: density measurements and the thermodynamics of O–S–Fe–Ni–Cu liquids at low to moderate pressures. Contrib. Mineral. Petrol. 156, 785–797.
Krogh-Moe, J., 1956. A method for converting experimental X-ray intensities to an absolute scale. Acta Crystallogr. 9, 951.
Kuwayama, K., Sawai, T., Hirose, K., Sata, N., Ohishi, Y., 2009. Phase relations of iron–silicon alloys at high pressure and high temperature. Phys. Chem. Miner. 36, 511–518.
Li, J., Fei, Y., Mao, H.K., Hirose, K., Shieh, S.R., 2001. Sulfur in the Earth's inner core. Earth Planet. Sci. Lett. 193, 509–514.
Luo, S.-N., Ahrens, T.J., 2004. Shock-induced superheating and melting curves of geophysically important minerals. Phys. Earth Planet. Inter. 143–144, 369–386.
McDonough, W.F., 2003. Compositional model for the Earth's core. Treatise in Geochemistry 2, 547–568.
Mezouar, M., Crichton, W.A., Bauchau, S., Thurel, F., Witsch, H., Torrecillas, F., Blattman, G., Marion, P., Dabin, Y., Chavanne, J., Hignette, O., Morawe, C., Borel, C., 2005. Development of a new state-of-the-art beamline optimized for monochromatic single crystal and powder X-ray diffraction under extreme conditions at the ESRF. J. Synch. Radiat. 12, 659–664.
Morard, G., Andrault, D., Guignot, N., Sanloup, C., Mezouar, M., Petitgirard, S., Fiquet, G., 2008a. In-situ determination of Fe–Fe_3S phase diagram and liquid structural properties up to 65 GPa. Earth Planet. Sci. Lett. 272, 620–626.
Morard, G., Andrault, D., Guignot, N., Siebert, J., Garbarino, G., Antonangeli, D., 2011. Melting of Fe–Ni–Si and Fe–Ni–S alloys at megabar pressures: implications for the Core–mantle boundary temperature. Phys. Chem. Miner. 38, 767–776.
Morard, G., Sanloup, C., Fiquet, G., Mezouar, M., Rey, N., Poloni, R., Beck, P., 2007. Structure of eutectic Fe–FeS melts up to 17 GPa: implications for planetary cores. Earth Planet. Sci. Lett. 263, 128–139.
Morard, G., Sanloup, C., Guillot, B., Fiquet, G., Mezouar, M., Perrillat, J.P., Garbarino, G., Mibe, K., Komabayashi, T., Funakoshi, K., 2008b. In situ structural investigation of Fe–S–Si immiscible liquid system and evolution of Fe–S bond properties with pressure. J. Geophys. Res. 113, B10205.
Nelder, J.A., Mead, R., 1965. A simplex method for function minimization. Comput. J. 7, 308.
Nishida, K., Terasaki, H., Ohtani, E., Suzuki, A., 2008. The effect of sulfur content on density of the liquid Fe–S at high pressure. Phys. Chem. Miner. 35, 417–423.
Norman, N., 1957. The Fourier transform method for normalizing intensities. Acta Crystallogr. 10, 370.
Ozawa, H., Hirose, K., Mitome, M., Bando, Y., Sata, N., Ohishi, Y., 2008. Chemical equilibrium between ferropericlase and molten iron to 134 GPa and implications for iron content at the bottom of the mantle. Geophys. Res. Lett. 35, 05308.
Pasek, M.A., Milsom, J.A., Ciesla, F.J., Lauretta, D.S., Sharp, C.M., Lunine, J.I., 2005. Sulfur chemistry with time-varying oxygen abundance during Solar System formation. Icarus 175, 1–14.
Poirier, J.P., 1994. Light elements in the Earth's outer core: a critical review. Phys. Earth Planet. Inter. 85, 319–337.
Rudge, J.F., Kleine, T., Bourdon, B., 2010. Broad bounds on Earth's accretion and core formation constrained by geochemical models. Nat. Geosci. 3, 439–443.
Sakai, T., Ohtani, E., Kamada, S., Terasaki, H., Hirao, N., 2012. Compression of $Fe_{88.1}Ni_{9.1}S_{2.8}$ alloy up to the pressure of Earth's inner core. J. Geophys. Res. 117, B02210.
Sanloup, C., Fiquet, G., Gregoryanz, E., Morard, G., Mezouar, M., 2004. Effect of Si on liquid Fe compressibility: implications for sound velocity in core materials. Geophys. Res. Lett. 31, L07604.
Sanloup, C., Guyot, F., Gillet, P., Mezouar, M., Martinez, I., 2000. Density measurements on liquid Fe–S alloys at high pressure. Geophys. Res. Lett. 27, 811–814.
Sata, N., Hirose, K., Shen, G., Nakajima, Y., Ohishi, Y., Hirao, N., 2010. Compression of FeSi, Fe3C, Fe0.95O, and FeS under the core pressures and implication for light element in the Earth's core. J. Geophys. Res. 115, B09204.
Schultz, E., Mezouar, M., Crichton, W.A., Bauchau, S., Blattman, G., Andrault, D., Fiquet, G., Boehler, R., Rambert, N., Sitaud, B., Loubeyre, P., 2005. Double-sided laser heating system for in situ high-pressure and high temperature monochromatic X-ray diffraction at the ESRF. High Pressure Res. 25, 71–83.
Shen, G., Rivers, M.L., Sutton, S.R., Sata, N., Prakapenka, V.B., Oxley, J., Suslick, K.S., 2004. The structure of amorphous iron at high pressures up to 67 GPa measured in diamond anvil cell. Phys. Earth Planet. Inter. 143–144, 481–495.
Siebert, J., Badro, J., Antonangeli, D., Ryerson, F.J., 2012. Metal–silicate partitioning of Ni and Co in a deep magma ocean. Earth Planet. Sci. Lett. 321–322, 189–197.
Siebert, J., Corgne, A., Ryerson, F.J., 2011. Systematics of metal-silicate partitioning for many siderophile elements applied to Earth's core formation. Geochim. Cosmochim. Acta 75, 1451–1489.
Sinmyo, R., Hirose, K., 2010. The Soret diffusion in laser-heated diamond-anvil cell. Phys. Earth Planet. Inter. 180, 172–178.
Souriau, A., Teste, A., Chevrot, S., 2003. Is there any structure inside the liquid outer core? Geophys. Res. Lett. 30, 1157.
Tateyama, R., Ohtani, E., Terasaki, H., Nishida, K., Shibazaki, Y., Suzuki, A., Kikegawa, T., 2011. Density measurements of liquid Fe–Si alloys at high pressure using the sink–float method. Phys. Chem. Miner. 38, 801–807.
Terasaki, H., Nishida, K., Shibazaki, Y., Sakamaki, T., Suzuki, A., Ohtani, E., Kikegawa, T., 2010. Density measurement of Fe3C liquid using X-ray absorption image up to 10 GPa and effect of light elements on compressibility of liquid iron. J. Geophys. Res. 115, B06207.
Wade, J., Wood, B.J., 2005. Core formation and the oxidation state of the Earth. Earth Planet. Sci. Lett. 236, 78–95.
Wade, J., Wood, B.J., Tuff, J., 2012. Metal–silicate partitioning of Mo and W at high pressures and temperatures: evidence for late accretion of sulphur to the Earth. Geochim. Cosmochim. Acta 85, 58–74.
Walker, D., Cranswick, L.M.D., Verma, P.K., Clark, S.M., Buhre, S., 2002. Thermal equations of state for B1 and B2 KCl. Am. Mineral. 87, 805–812.
Waseda, Y., 1980. The Structure of Non-Crystalline Materials. McGraw-Hill International Book Company.